Desalination and Water Treatment
www.deswater.com
doi: 10.5004/dwt.2022.29073

279 (2022) 85–89
December

Large eddy simulation of turbulent flow of pseudoplastic and dilatant fluids: rheological and hydrodynamic behaviour

Mohamed Abdi[a,*], Khaled Chaib[a], Meryem Ould-Rouiss[b], Slimane Benferhat[a]

[a]*Laboratoire de génie électrique et des plasmas (LGEP) University of Tiaret, Algeria, email: abdi.mohamed1@live.fr (M. Abdi)*
[b]*Laboratoire de Modélisation et Simulation Multi Echelle, MSME, Université Gustave Eiffel, UMR 8208 CNRS, 5 bd Descartes, 77454 Marne-la-Vallée, Paris, France*

Received 19 April 2022; Accepted 27 September 2022

ABSTRACT

A fully developed turbulent pipe flow of non-Newtonian fluids was investigated numerically using the large eddy simulation (LES) method. The present investigation mainly focuses on the rheological and hydrodynamic behaviour of the pseudoplastic (shear-thinning) and dilatant (shear-thickening) fluids over a wide range of flow behaviour indexes 0.75, 0.8, 1, 1.2, 1.4, and 1.6 at a simulation Reynolds number of 12,000. The computations are based on a finite difference scheme, second-order accurate in space and time. The numeric resolution is 65^3 grid points in r, θ and z directions, respectively. According to the results, the shear rate profiles of the pseudoplastic decreased while the dilatant fluid improved with a higher flow index along the pipe radius. Additionally, the elevated flow index caused a rise in the fluid viscosity close to the wall, which raised the friction factor.

Keywords: LES; Shear-thinning; Shear-thickening; Fully developed; Turbulent flow

1. Introduction

Numerous industrial applications have emerged that enhance technology in the flow of non-Newtonian fluids. These fluids are used in various technical applications, including cement and paint production, oil field operations, the petroleum, pharmaceutical, and polymer processing industries, transportation, and food and polymer solutions. Over the past few decades, there has been an increasing interest in the turbulent flow of non-Newtonian fluids through axial pipes. Various experimental, theoretical, and numerical studies have been conducted to understand how the fluids' rheological properties affect the hydrodynamic and thermal characteristics. The flow of power-law fluids in an isothermal axial pipe has been studied in a significant quantity of literature, either experimentally [1–6] or numerically [7–13].

One of the critical studies to fill in the gap and advance understanding was that of Gavrilova and Rudyak [11,12]. They conducted direct numerical simulations (DNS) at two generalised Reynolds values, 10,000 and 20,000, over the power-law index 0.4–1. The authors presented the distributions of Reynolds stress tensor components, averaged viscosity, viscosity fluctuations, and measures of turbulent anisotropy in 2016 [11], concentrating on turbulent mean values. The identical research was described a year later [12]. But this time, they presented the distributions of the turbulent stress tensor components and the shear stress and turbulent kinetic energy balances, focusing on the energy balance and the shear stresses. To understand how shear thinning or thickening affects first and second-order flow statistics, including turbulent kinetic energy production, transport, and dissipation in such flows, Singh et al. [13] recently investigated the effect of the flow index parameter of power-law fluids in turbulent pipe flow using direct numerical simulation at a friction Reynolds number $Re_\tau = 323$.

* Corresponding author.

Presented at the First International Congress of Energy and Industrial Process Engineering (ICEIPE'22) 23–25 May 2022, Algiers, Algeria

More recently, Abdi et al. [14] have conducted a fully developed turbulent forced convection of thermally independent pseudoplastic fluid with a flow behaviour index of 0.75 through an axially heated rotating pipe, by means of LES with an extended Smagorinsky model. With a rotation rate ranging from 0 to 3, the simulation Reynolds and Prandtl numbers of the working fluid were assumed to be 4,000 and 1, respectively. It is observed that as the pipe wall rotates, it is seen that the temperature along its radius noticeably decreases as the rotation rate increases. This is because the apparent fluid viscosity in the pipe's core region decreases, which causes a centrifugal force that causes the mean axial velocity profile to increase noticeably.

The present investigation focuses numerically on the fully developed turbulent flow of power-law fluids in an axially stationary pipe using a large eddy simulation (LES) with a standard dynamic model. The flow behaviour index was set to 0.75, 0.8, 1, 1.2, 1.4, and 1.6 at a simulation Reynolds number of 12,000. The specific objective of the present investigation is to discern the effects of the flow behaviour index of the shear-thinning and shear-thickening fluids on different fluid rheological characteristics and hydrodynamic properties to describe the turbulent flow patterns and rheological behaviour of this kind of non-Newtonian fluid.

2. Governing equations and numerical procedure

2.1. Governing Equations

The present study deals numerically with a fully developed turbulent flow of power-law fluids in a pipe at different flow behaviour indexes ($0.75 \le n \le 1.6$) at a simulation Reynolds number of 12,000, employing the LES approach with a standard dynamic model, with a computational domain length of $20R$ (Fig. 1). The filtered equations were expressed as Eqs. (1) and (2):

$$\frac{\partial \overline{u}_i}{\partial x_i} = 0 \tag{1}$$

$$\frac{\partial \overline{u}_j}{\partial t} + \frac{\partial \overline{u}_i \overline{u}_j}{\partial x_i} = -\frac{d\overline{P}}{\partial x_j} + \frac{1}{\mathrm{Re}_s}\frac{\partial}{\partial x_i}\left[\overline{\dot{\gamma}^{n-1}}\left(\frac{\partial \overline{u}_j}{\partial x_i} + \frac{\partial \overline{u}_i}{\partial x_j}\right)\right] + \frac{\partial \overline{\tau}_{ij}}{\partial x_i} \tag{2}$$

where $\mathrm{Re}_s = \rho U_{CL}^{2-n} R^n / K$ is the simulation Reynolds number, where (U_{CL}) is the centreline axial velocity of the analytical fully developed laminar profile and is defined as $U_{CL} = (3n + 1)U_b/(n + 1)$. The constitutive equation for the power-law model is given by:

$$\tau = K\dot{\gamma}^n \tag{3}$$

The variables K and n are the fluid consistency index and the flow behaviour index, respectively. The shear-thinning behaviour occurs for $n < 1$, shear-thickening for $n > 1$, and $n = 1$ the fluid shows Newtonian behaviour.

2.2. Numerical procedure

In the non-Newtonian Smagorinsky model, the subgrid stress tensor $\overline{\tau}_{ij}$ is linked to the strain rate tensor by $\overline{\tau}_{ij} = 2v_t\overline{s}_{ij}$. The turbulent viscosity is computed by $v_t = C_s f_s \left(f_n \Delta\right)^2 \overline{s}_{ij}$, where Δ is the computational filter, C_s the model constant, f_s the van Driest wall damping function, and f_n is the correction function for the change in viscosity.

A no-slip boundary condition was applied at the pipe wall to perform a realistic numerical simulation, and a periodic boundary condition was applied in the axial and circumferential directions. As for the grid resolution, a grid of 65^3 grid points in axial, radial, and circumferential directions, respectively, was found to provide an accurate prediction of the rheological and hydrodynamic characteristics, in agreement with the available data of the literature and to give a good compromise between the required CPU-time and accuracy. Moreover, a uniform computational grid was utilised for the axial and circumferential directions, while a non-uniform mesh specified by a hyperbolic tangent function was applied in the radial direction.

3. Results and discussion

The present section largely analyses and discusses the mean quantities and the rheological properties, such as the evolution of the apparent fluid viscosity, the shear stress, the shear rate, the mean axial velocity, and the friction factor. This section seeks to explore the effect of the flow behaviour index of the power-law fluid on the rheological and hydrodynamic properties to describe the turbulent flow pattern and rheological behaviour of this kind of non-Newtonian fluid in the present computational domain.

3.1. Validation

The findings were compared with DNS data available in the literature to ascertain the accuracy and reliability of the predicted results of the LES laboratory code. Fig. 2 compares the turbulent axial velocity of a shear-thinning fluid with a flow behaviour index of 0.75 at a Metzner Reed Reynolds number of 4,255 with a direct numerical

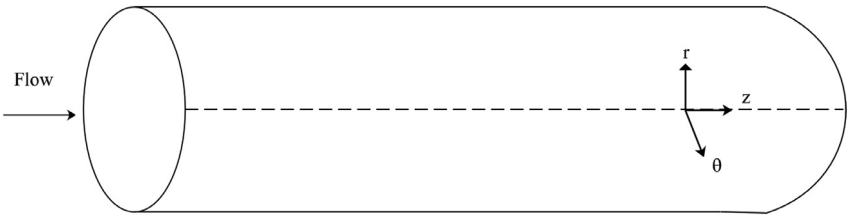

Fig. 1. Computational domain.

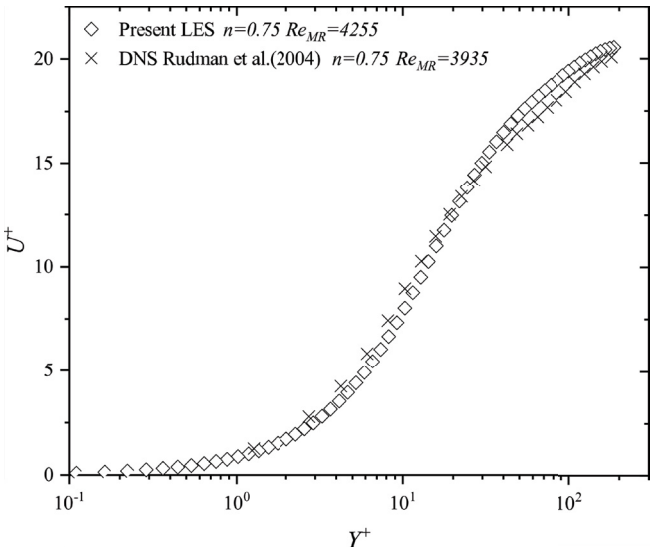

Fig. 2. Validation of the present results.

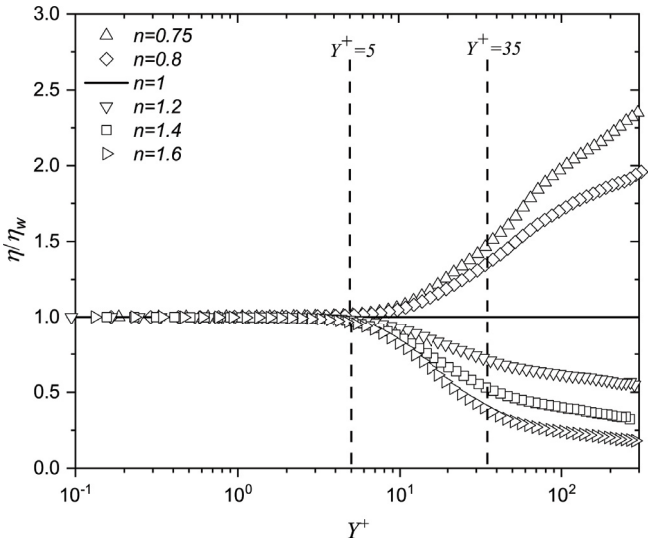

Fig. 3. Apparent viscosity profile of the pseudoplastic, Newtonian, and dilatant fluids vs. Y^+.

simulation flow behaviour index of 0.75 at Metzner Reed Reynolds number of 3,935 [8]. It should be said that no significant noteworthy differences were observed, where the predicted profile almost coincides with that of DNS data [8] along flow regions. There is a minor discrepancy in the logarithmic region because of the difference in the Reynolds number value and the numerical solution procedure.

The increase in shear-thinning (i.e., decreasing n) and the rise in shear-thickening (i.e., increasing n) resulted in a marked attenuation and enhancement in the shear rate, respectively, along the pipe radius, especially in the near-wall region. It should be noted that for the pseudoplastic fluids, the increased flow behaviour index leads to a noticeable reduction in the shear rate along the pipe radius: the flow behaviour index increased as the shear rate was attenuated. In contrast, for dilatant fluids, the increased flow behaviour index induced a significant enhancement of the shear rate along the pipe radius: the flow behaviour index increased as the shear rate was enhanced.

As shown in Fig. 3, the apparent viscosity of the Newtonian fluid was linear along the pipe radius and equalled the apparent viscosity at the wall (η_w) In turn, the apparent viscosity of the shear-thinning and shear-thickening fluids were identical and equal to the viscosity at the wall along the viscous sublayer ($0 \le Y^+ \le 5$) for all flow behaviour indices. The flow behaviour index significantly affected the apparent viscosity of the shear-thinning and shear-thickening fluids in the near-wall region, where the increased flow index yielded to enhancement in the fluid viscosity in the viscous sublayer.

The apparent viscosity of the power-law profiles deviated significantly from each other, only starting from the buffer region; this deviation became more distinct with distance away from the wall toward the core region for all flow behaviour indices. Beyond $Y^+ = 5$, the apparent viscosity of the pseudoplastic fluids enhanced gradually with the distance from the wall toward the core region; it was evident that the as the flow behaviour index (n) decreased significantly as the pseudoplastic apparent viscosity increased in the logarithmic region ($30 \le Y^+ \le 200$). In contrast, the apparent viscosity of the dilatant fluids was attenuated gradually with distance from the wall (Y^+) towards the core region. The increased flow behaviour index (n) yielded a marked reduction in the apparent viscosity of the viscous sublayer, especially in the logarithmic region. It should be noted that with decreasing flow behaviour index, the pseudoplastic and dilatant fluids tended to behave like solids when approaching the pipe centre. These fluids behaved like liquids rather than solids, with an increasing flow behaviour index approaching the pipe core region.

Fig. 4 depicts the apparent viscosity profiles scaled by the viscosity at the wall (η_w) of the shear-thinning and shear-thickening fluids against the shear rate scaled by the shear rate at the wall (γ_w). The apparent viscosity of the Newtonian fluid was constant along the pipe radius. It equalled the wall viscosity, which means the Newtonian apparent viscosity was independent of the flow shear rate. As observed in Fig. 4, the apparent viscosity of the power-law profiles deviated significantly from each other, only starting from the buffer region; this deviation became more distinct with distance away from the wall toward the core region for all flow behaviour indices. Beyond $Y^+ = 5$, the apparent viscosity of the pseudoplastic fluids increases gradually with the distance. As observed in Fig. 4, the apparent viscosity of the non-Newtonian fluids was not constant where it was a function of the shear rate, where the apparent viscosity of the pseudoplastic and dilatant fluids varied with the shear rate along the pipe radius. It was evident that the shear rate attenuated gradually from the wall towards the core region for all flow behaviour indices (Fig. 5), where this decreased shear rate resulted in a marked enhancement and reduction in the apparent viscosity of the shear-thinning and shear-thickening (Fig. 3). This trend was more pronounced as the flow behaviour index (n) increased. It should also be noted that this finding confirmed the association between the apparent fluid viscosity and the power-law fluids' shear rate $\eta = K\dot{\gamma}^{n-1}$.

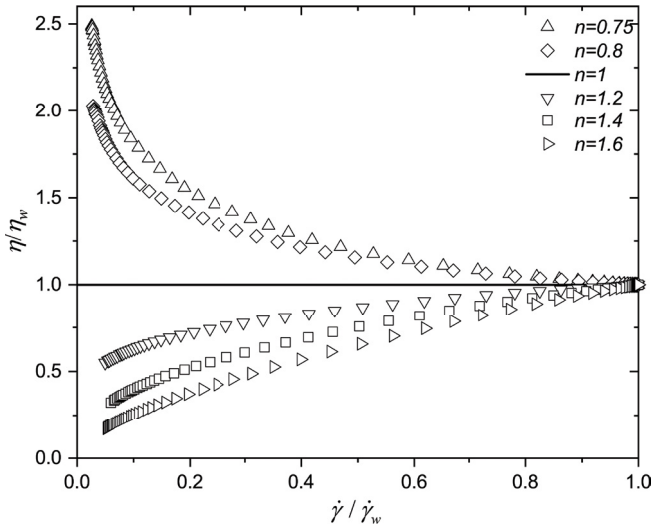

Fig. 4. Apparent viscosity of the pseudoplastic, Newtonian, and dilatant fluids vs. shear rate.

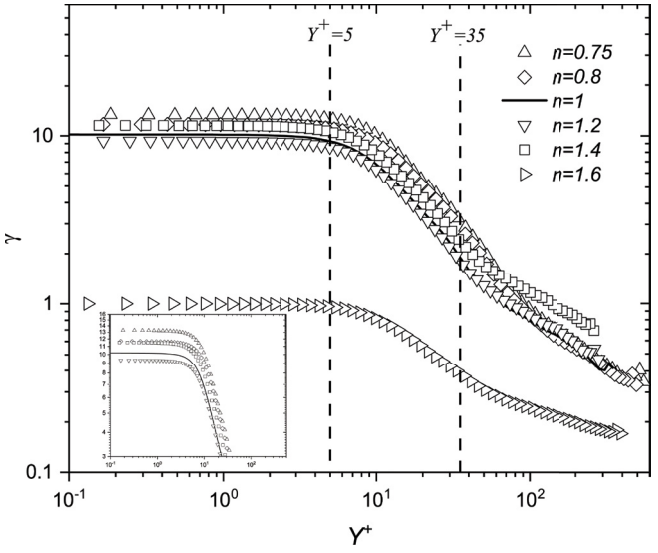

Fig. 5. Shear rate profile of the pseudoplastic, Newtonian, and dilatant fluids against the Y^+.

3.2. Axial velocity profiles

Fig. 6 illustrates the turbulent axial velocity profile scaled by the friction velocity vs. the distance from the wall in wall units Y^+ of the shear-thinning and shear-thickening fluids. The flow behaviour index was chosen to be 0.75, 0.8 (shear-thinning) and 1.2, 1.4, 1.6 (shear-thickening) in addition to the Newtonian fluid (n = 1) at a same simulation Reynolds number (Re_s = 12,000). Where the dash lines represented the universal velocity distributions in the viscous sublayer ($0 \le Y^+ \le 5$) and in the logarithmic layer ($30 \le Y^+ \le 200$).

As shown in Fig. 6, the turbulent axial velocity profile of the Newtonian fluid agreed entirely with the universal linear ($U^+ = Y^+$) and logarithmic ($U^+ = 2.5\ln Y^+ + 5.5$) laws in the viscous sublayer and logarithmic layer, respectively. As for the power-law fluids, the turbulent axial velocity

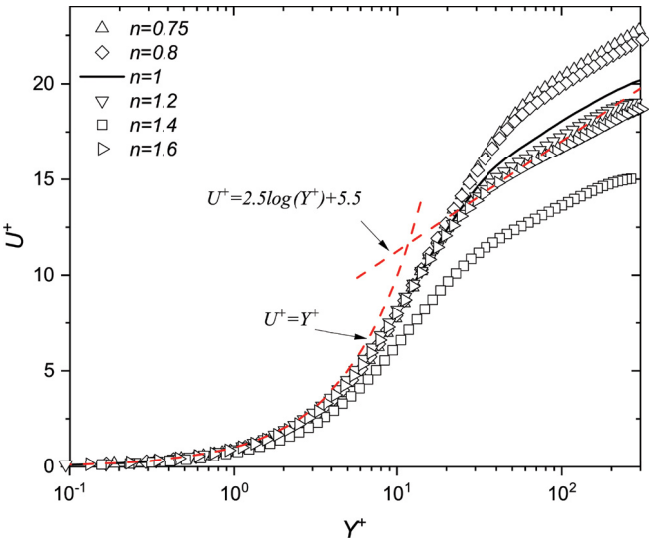

Fig. 6. Turbulent axial velocity profile of the pseudoplastic, Newtonian, and dilatant fluids.

profiles of the pseudoplastic (n < 1) and dilatant (n > 1) fluids were identical for all flow behaviour indices in the viscous sublayer, where they were also in good agreement with the universal linear ($U^+ = Y^+$) in the vicinity of the wall up to approximately (Y^+ = 10). It can be said that the mean axial velocity was almost independent of the flow behaviour index in this flow region.

Further away from the pipe wall, the effect of the flow behaviour index began to become apparent with the distance from the wall (Y^+), and the turbulent axial velocity profiles of the pseudoplastic and dilatant fluids deviated significantly from each other beyond (Y^+ = 20) with the distance from the wall. Away from the wall towards the pipe centre, this deviation was more pronounced in the logarithmic layer ($30 \le Y^+ \le 200$), where this discrepancy was attributed to the influence of the apparent viscosity and the shear rate of the power-law fluids in this region.

It can be seen from Fig. 6 that the turbulent axial velocity profiles of the shear-thinning fluids were somewhat larger than the Newtonian one, where the pseudoplastic profiles lay above the corresponding Newtonian fluid in the logarithmic layer. In contrast, the turbulent axial velocity profiles of the shear-thickening fluids lay down the Newtonian one in this region. It should be noted that the decrease in the flow behaviour index resulted in an enhancement in the turbulent axial velocity profile with distance from the wall (Y^+) away from the wall towards the logarithmic region, where this trend was more pronounced as the flow behaviour index (n) decreased.

3.3. Friction factor

As seen in Table 1, the friction factor (f) enhanced monotonically with the flow behaviour index (n); it can be said that the increased flow behaviour index results in a marked enhancement in the friction factor for the pseudoplastic and dilatant fluids. This discrepancy was attributed to the influence of the apparent fluid viscosity: the high apparent

Table 1
Friction factor

n	f E-01
0.75	0.0819
0.8	0.0845
1	0.108
1.2	0.125
1.4	0.141
1.6	0.147

viscosity at the wall increased the friction factor. As the flow behaviour index rose as the apparent fluid viscosity was enhanced (Fig. 4), the friction factor was also improved (Table 1).

4. Conclusions

The numerical analysis of the fully developed turbulent flow of pseudoplastic and dilatant fluids in an isothermal stationary pipe using a large eddy simulation and a conventional dynamic model was presented in this work over a wide range of flow behaviour indexes 0.75, 0.8, 1, 1.2, 1.4, and 1.6 at a simulation Reynolds number of 12,000.

The results showed that when the flow behaviour index was raised, the shear rate attenuated, which resulted in a notable drop in the shear rate profile throughout the pipe radius for pseudoplastic fluids. On the other hand, for dilatant fluids, an increase in the flow behaviour index resulted in a significant amplification in the shear rate throughout the pipe radius; that is, as the flow behaviour index rose, so did the shear rate. The apparent viscosity of the pseudoplastic fluids increased away from the pipe wall as the flow behaviour index decreased, and the fluid tended to behave like a solid as it got closer to the pipe core area. When approaching the pipe core area, the fluid behaved more like a liquid, whereas the apparent viscosity of the dilatant fluids progressively decreased with distance from the wall. This tendency was more noticeable in the flow behaviour index. Likewise, when reaching the pipe core region, the pseudoplastic and dilatant fluid acted like a solid and a liquid, respectively. The shear rate increased as it moved out of the viscous sublayer through the remaining flow regions. Particularly in the logarithmic region, the turbulent axial velocity of the shear-thinning fluid was greater than that of the shear-thickening fluid; this tendency became more pronounced as the flow behaviour index was reduced. This discrepancy was related to the power-law fluids' apparent viscosity and shear rate in this region. Finally, due to a higher flow behaviour index, the apparent fluid viscosity close to the wall was significantly enhanced, which raised the friction factor.

Symbols

U_b — Average velocity, m·s^{-1}
U_τ — Friction velocity $U_\tau = (\tau_w/\rho)^{1/2}$, m·s^{-1}
U_{CL} — Centreline axial velocity for analytical fully developed laminar profile $U_{CL} = (3n + 1)U_b/(n + 1)$, m·s^{-1}
R — Pipe radius, m
n — Flow index
K — Consistency index, Pa·s^n
Y^+ — Wall distance $Y^+ = \rho U_\tau Y/\eta_w$
f — Friction factor $f = 2\tau_w/(\rho U_b^2)$
Re_s — Reynolds number of the simulations $\mathrm{Re}_s = \rho U_{CL}^{2-n} R^n/K$

Greek symbols

$\dot{\gamma}$ — Shear rate $\dot{\gamma} = \sqrt{S_{ij}S_{ij}}$
η — apparent viscosity $\eta = K\dot{\gamma}^{n-1}$
ρ — Density
$\bar{\tau}_{ij}$ — Subgrid stress tensor $\bar{\tau}_{ij} = -2\nu_t \bar{S}_{ij}$

Subscripts

z, r, θ — Axial, radial, tangential velocity
C — Centreline
L — Laminar
s — Simulation
w — Wall

Superscripts

$\langle\ \rangle$ — Statistically averaged
$(\ )^+$ — Normalised by U_τ

References

[1] A.B. Metzner, J.C. Reed, Flow of non-Newtonian fluids—correlation of the laminar, transition, and turbulent-flow regions, AlChE J., 1 (1955) 434–440.
[2] A.B. Metzner, Non-Newtonian fluid flow. Relationships between recent pressure-drop correlations, Ind. Eng. Chem., 49 (1957) 1429–1432.
[3] D.W. Dodge, A.B. Metzner, Turbulent flow of non-Newtonian systems, AlChE J., 5 (1959) 189–204.
[4] Y. Tomita, A study on non-Newtonian flow in pipe lines, Bull. JSME, 2 (1959) 10–16.
[5] V. Vidyanidhi, A. Sithapathi, Non-Newtonian flow in a rotating straight pipe, J. Phys. Soc. Jpn., 29 (1970) 215–219.
[6] F.T. Pinho, J.H. Whitelaw, Flow of non-Newtonian fluids in a pipe, J. Non-Newtonian Fluid Mech., 34 (1990) 129–144.
[7] M.R. Malin, Turbulent pipe flow of power-law fluids, Int. Commun. Heat Mass Transfer, 24 (1997) 977–988.
[8] M. Rudman, H.M. Blackburn, L.J.W. Graham, L. Pullum, Turbulent pipe flow of shear-thinning fluids, J. Non-Newtonian Fluid Mech., 118 (2004) 33–48.
[9] T. Ohta, M. Miyashita, DNS and LES with an extended Smagorinsky model for wall turbulence in non-Newtonian viscous fluids, J. Non-Newtonian Fluid Mech., 206 (2014) 29–39.
[10] P.S. Gnambode, P. Orlandi, M. Ould-Rouiss, X. Nicolas, Large-Eddy simulation of turbulent pipe flow of power-law fluids, Int. J. Heat Fluid Flow, 54 (2015) 196–210.
[11] A.A. Gavrilov, V.Y. Rudyak, Direct numerical simulation of the turbulent flows of power-law fluids in a circular pipe, Thermophys. Aeromech., 23 (2016) 473–486.
[12] A.A. Gavrilov, V.Ya. Rudyak, Direct numerical simulation of the turbulent energy balance and the shear stresses in power-law fluid flows in pipes, Fluid Dyn., 52 (2017) 363–374.
[13] J. Singh, M. Rudman, H.M. Blackburn, The effect of yield stress on pipe flow turbulence for generalised Newtonian fluids, J. Non-Newtonian Fluid Mech., 249 (2017) 53–62.
[14] M. Abdi, A. Noureddine, M. Ould-Rouiss, Numerical simulation of turbulent forced convection of a power law fluid flow in an axially rotating pipe, J. Braz. Soc. Mech. Sci., Eng., 42 (2020) 17.